HYDROLOGICAL PROCESSES
Hydrol. Process. **25**, 2439–2455 (2011)
Published online 2 March 2011 in Wiley Online Library
(wileyonlinelibrary.com) DOI: 10.1002/hyp.8021

Study of stream temperature dynamics and corresponding heat fluxes within Miramichi River catchments (New Brunswick, Canada)

Cindie Hebert,[1] Daniel Caissie,[2]* Mysore G. Satish[1] and Nassir El-Jabi[3]

[1] *Faculty of Engineering, Dalhousie University, Halifax, NS, B3J 2X4, Canada*
[2] *Fisheries and Oceans, Moncton, NB, E1C 9B6, Canada*
[3] *Faculty of Engineering, Université de Moncton, Moncton, NB, Canada*

Abstract:

Water temperature is a key physical habitat determinant in lotic ecosystems as it influences many physical, chemical, and biological properties of rivers. Hence, a good understanding of the thermal regime of rivers and river heat fluxes is essential for effective management of water and fisheries resources. This study dealt with the modelling of river water temperature using a deterministic model. This model calculated the different heat fluxes at the water surface and from the streambed using different hydrometeorological conditions. The water temperature model was applied on two watercourses of different sizes and thermal characteristics, but within a similar meteorological region, namely, the Little Southwest Miramichi River and Catamaran Brook (New Brunswick, Canada). The model was also applied using microclimate data, i.e. meteorological conditions within the river environment (1–2 m above the water surface), for a better estimation of river heat fluxes. Water temperatures at different depths within the riverbed were also used to estimate the streambed heat fluxes. Results showed that microclimate data were essential to get accurate estimates of the surface heat fluxes. Results also showed that for larger river systems, the surface heat fluxes were generally the dominant component of the heat budget with a correspondingly smaller contribution from the streambed. As watercourses became smaller and groundwater contribution more significant, the streambed contribution became important. For instance, approximately 80% of the heat fluxes occurred at the surface for Catamaran Brook (20% from the streambed) whereas the Little Southwest Miramichi River showed values closer to 90% (10% from the streambed). As was reported in previous studies, the solar radiation input dominated the contribution to the heat gain at 63% for Catamaran Brook and 89% for Little Southwest Miramichi River. Copyright © 2011 John Wiley & Sons, Ltd.

KEY WORDS river; stream; water temperature; modeling; streambed; heat fluxes

Received 22 October 2009; Accepted 20 January 2011

INTRODUCTION

Water temperature has both economic and ecological significance when considering issues such as water quality and biotic conditions in rivers (Caissie, 2006). As such, fish habitat suitability is highly dependant on stream water temperatures. The thermal regime of rivers is influenced by many factors such as atmospheric conditions, topography, riparian vegetation, stream discharge, and streambed thermal fluxes (Poole and Berman, 2001; Caissie, 2006; Webb *et al*., 2008). It is therefore important to use adequate water temperature modelling approaches to effectively predict water temperature variability.

Stream water temperatures have been studied for many years (Macan, 1958; Raphael, 1962; Brown, 1969). Water temperature controls the rate of decomposition of organic matter, dissolved oxygen content, and chemical reactions in general. Stream water temperature can also impact recreational activities such as swimming and fishing. Early studies have mainly focused on the impact of forest harvesting on water temperature, whereas recent studies are also focusing on fish habitat-related issues. For example, studies have found that stream water temperature dynamics can influence many fish habitat conditions including the growth rate of fishes, aquatic invertebrates, and others (Markarian, 1980; Wichert and Lin, 1996; Beitinger and Bennett, 2000; Cox and Rutherford, 2000a, 2000b). Stream temperatures have also been monitored in order to evaluate the impact of human activities due to urbanisation (Kinouchi *et al*., 2007; Nelson and Palmer, 2007), thermal pollution (Bradley *et al*., 1998) as well as land-use activities (Nagasaka *et al*., 1999). Flow reduction and flow alteration have also been observed to have an impact on the thermal regime of rivers (Morin *et al*., 1994; Sinokrot and Gulliver, 2000). Understanding of the thermal regime of rivers in forested ecosystems has played an important role in the development of water temperature models, as valuable information was learned from heat exchange processes, such as the contribution by solar radiation, conduction, and others (Sridhar *et al*., 2004; Moore et *al*., 2005). However, increased interest has been noted recently due to the potential effects of climate change on river thermal regimes (Morrison *et al*., 2002; Morrill *et al*., 2005; Tung *et al*., 2006).

* Correspondence to: Daniel Caissie, Fisheries and Oceans, Moncton, NB, E1C 9B6, Canada. E-mail: Daniel.Caissie@dfo-mpo.gc.ca

Water temperature models can be classified into two groups: deterministic or statistical. The statistical approach predicts water temperatures by linking water temperatures to relevant meteorological parameters, usually air temperature (Sinokrot and Stefan, 1993; Caissie *et al*., 2001; Ahmadi-Nedushan *et al*., 2007). The major drawback of this approach lies in the lack of explanation of underlying physical processes. Deterministic models are often used instead of statistical models because they consider cause and effect relations between meteorological parameters and river water temperatures (Raphael, 1962; Morin and Couillard, 1990; Morin *et al*., 1994). Deterministic models are also among the most widely used models for predicting river water temperatures (Evans *et al*., 1998; Younus *et al*., 2000; Caissie *et al*., 2007; Hannah *et al*., 2008). This energy-budget model (based on conservation of energy) estimates changes in river water temperature from energy fluxes at two levels, namely at the stream water-surface interface and at the streambed-water interface (or stream bottom). Energy components considered at the water surface generally include solar radiation, net long-wave radiation, evaporative, and sensible heat fluxes, whereas streambed heat fluxes mainly consist of heat conduction and advective heat fluxes (e.g. due to groundwater flow). A number of studies have used heat budget models to predict variability in river water temperatures (Evans *et al*., 1998; Younus *et al*., 2000; Caissie *et al*., 2007; Hannah *et al*., 2008); however, few have focused on using stream microclimate conditions as well as the streambed heat fluxes in predicting water surface heat fluxes. As such, the present study will focus on both these important issues.

A previous study was conducted within the same region using a deterministic model (Caissie *et al*., 2007). This previous study used remote meteorological data to predict stream water temperatures on a daily basis. The present study differs from Caissie *et al*. (2007) in that microclimate meteorological data were used to better estimate heat fluxes and potentially improve the modelling. Also, the modelling was carried out hourly rather than daily. Stream microclimate conditions (i.e. data collected 1–2 m above the stream) are important to properly estimate water surface heat fluxes, as they better represent conditions within the river environment. Streambed fluxes are also important to the thermal regime of rivers and they have not been thoroughly investigated within the literature (Caissie *et al*., 2007). Those who have considered streambed heat fluxes have reported that they were mostly important when modelling diel variability, e.g. hourly modelling (Sinokrot and Stefan, 1993; Hondzo and Stefan, 1994; Kim and Chapra, 1997; Webb and Zhang, 1997; Evans *et al*., 1998), and for shallow streams (Jobson, 1977).

The objective of the present study is to examine in detail the relative contribution of surface *versus* streambed heat fluxes of two watercourses under varied meteorological conditions. The specific objectives of the present study are: 1) to develop a heat budget model for two thermally different rivers (Catamaran Brook and Little Southwest Miramichi River, New-Brunswick, Canada) using stream microclimate data, 2) to compare observed *versus* predicted total heat fluxes for these watercourses, and 3) to compare the relative contribution of heat fluxes at both the air-water interface and at the water-streambed interface.

STUDY SITE

In many water temperature studies, meteorological data are usually taken from the nearest meteorological station (e.g. nearest airport), which can be kilometres away from the stream environment. As such, significant differences can exist between meteorological conditions at a remote station *versus* those experienced within the river environment (stream microclimate conditions). To truly understand energy fluxes within rivers, it is best to collect data at the microclimate scale, when possible. In the present study, data were collected within the stream environment at two microclimate sites. A remote meteorological station (within a cleared area of the forest) was also present within the study area. This station was only used to compare microclimate *versus* remote meteorological data for selected parameters (e.g. air temperature, wind speed, etc.).

The two studied watercourses are located within the Miramichi River system (New Brunswick, Canada), which is world renowned for its population of Atlantic salmon (Figure 1). This system has an annual precipitation ranging from 860 to 1365 mm, with a long-term average of 1142 mm (Caissie and El-Jabi, 1995). Mean monthly air temperature varies between −11·8 °C (January) and 18·8 °C (July). The mean annual runoff was estimated at 714 mm, ranging from 631 to 763 mm. The vegetation consists mainly of second-growth, mature forest species estimated at 65% coniferous and 35% deciduous (Cunjak *et al*., 1990).

The first study site was located on the Little Southwest Miramichi River (LSWM) at approximately 25 km from the river mouth (Figure 1). The second study site was located on Catamaran Brook (Cat Bk) approximately 8 km upstream of the mouth (Figure 1). Catamaran Brook is the site of a multidisciplinary hydrobiological research study aimed at quantifying stream ecosystem processes and the impact of timber harvesting (Cunjak *et al*., 1990). No lateral variation of water temperatures were observed at both LSWM and Cat Bk due to the well mixed nature of these rivers (Caissie *et al*., 2007). Site characteristics for both studied streams are listed in Table I.

Data collection

Meteorological stations were installed within the stream environment in Catamaran Brook and Little Southwest Miramichi River to monitor stream microclimate conditions (air temperature, relative humidity, wind speed, solar radiation, and water temperature). Sensors were installed approximately 2 m above the water surface

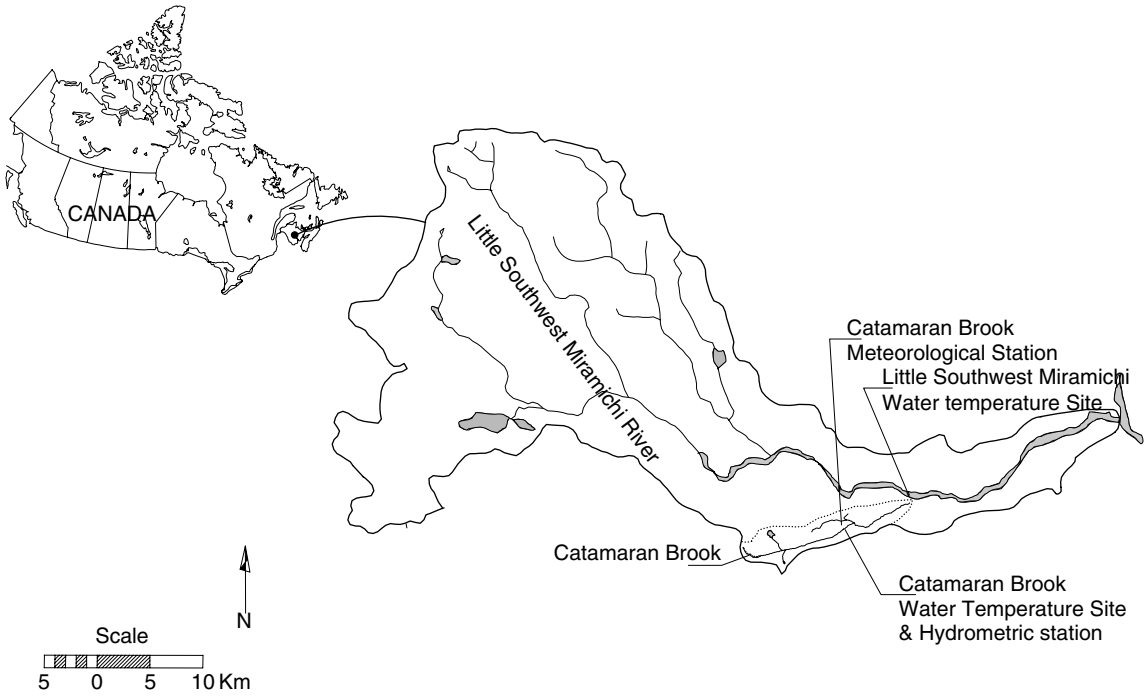

Figure 1. Map showing the location of microclimate sites (Catamaran Brook and Little Southwest Miramichi River) and the location of the remote meteorological station

Table I. Study site characteristics of Catamaran Brook and Little Southwest Miramichi River

Study site	Drainage area	Width	Depth	Canopy closer	Forest Composition	
					Hardwood	Softwood
Little Southwest Miramichi R.	1190 Km^2	80 m	0.55 m	20%	70	30
Catamaran Brook	27 Km^2	9 m	0.21 m	55–65%	60	40

and all sensors were scanned every 5 s by a CR10 (Campbell Scientific Corp.) data logger and hourly averages were then calculated. Water temperature was recorded using 107B Water Temperature sensors (Campbell Scientific Corps.). Air temperature and relative humidity were measured using a Vaisala Relative Humidity and Temperature sensor, whereas wind speed was monitored with a RM Young sensor. Solar radiation was measured using a Kipp and Zonen Silicon Pyranometer (at LSWM) and a LI-COR Silicon Pyranometer (at Cat Bk, and Met Sta sites).

Precipitation and barometric pressure were obtained from the Catamaran Brook meteorological station, which is located 1 km (Cat Bk) and 8 km (LSWM) from the stream microclimate sites. This remote station is located in the middle of a 400 m × 400 m clear-cut area. A tipping bucket rain gauge (model TE252M) was used to monitor precipitation at approximately 1·2 m from the ground and sheltered by an Alter-type wind shield. Daily mean discharges and hourly cloud cover were obtained from Environment Canada's hydrometric stations (01BP001 and 01BP002) and local weather station (Miramichi station 8 100 989). Mean water depth was obtained from discharge and a power function as described in Caissie *et al.* (2007). Streambed sensors were installed during the summer of 2007 at different depths, up to 3 m within the substrate at some sites, to monitor streambed temperatures.

Hourly data were collected at both microclimate sites (i.e. Catamaran Brook and Little Southwest Miramichi River) from 4 July 2007 (day 185) to 2 October 2007 (day 275) for the analysis of river heat fluxes. Within this period, six different periods were carefully selected to represent varied water temperature patterns and meteorological conditions to allow examination of different thermal regime conditions (Figure 2). For instance, Period 1 represents a period with the highest air and water temperatures during the summer (Table II). Period 2 was selected because it reflects generally clear sky conditions, and during this period air temperature generally decreased while water temperature increased. Period 3 represents low flow conditions with increasing air temperatures. To contrast Period 2, Period 4 was mostly cloudy with an important amount of precipitation (35·3 mm). Period 5 represents variable air and water temperatures, with air temperatures ranging between −1 and 26 °C. Period 6 represents autumn conditions with low solar radiation input (<100 W m^{-2}) and generally colder mean air temperatures (<14 °C).

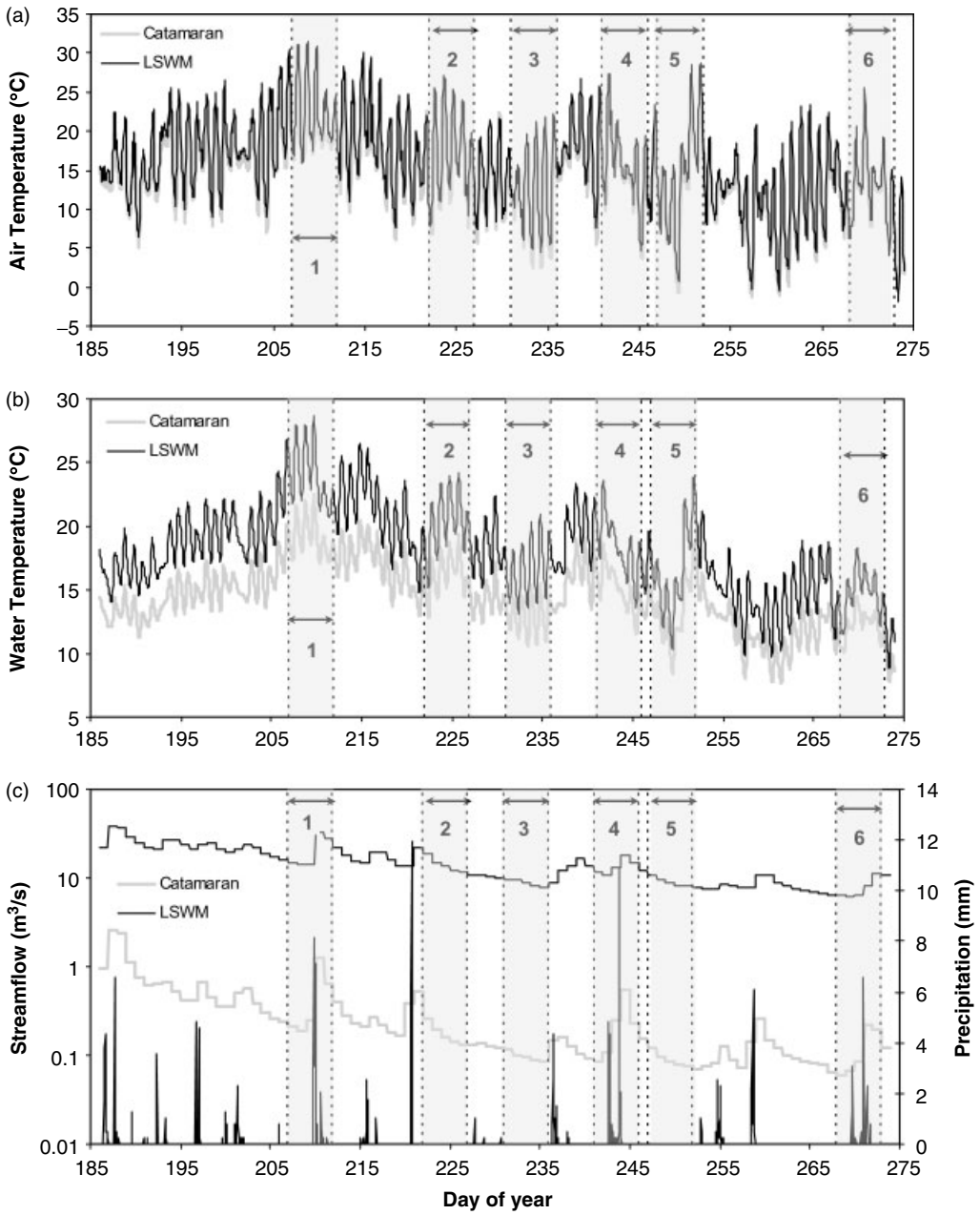

Figure 2. Time series plot of selected parameters (air temperature, water temperature, streamflow and precipitation) and study periods for both Catamaran Brook and Little Southwest Miramichi River. The stepped data in Figure 2c) represents daily mean discharge

METHODOLOGY

Heat budget

The modelling of stream water temperature has been carried out in previous studies using the heat budget approach (Sinokrot and Stefan, 1993; Caissie *et al.*, 2007). This modelling approach uses the general equation of conservation of thermal energy given by

$$\frac{\delta T_w}{\delta t} + v_x\frac{\delta T_w}{\delta x} + v_y\frac{\delta T_w}{\delta y} + v_z\frac{\delta T_w}{\delta z} - \frac{1}{A}\frac{\delta}{\delta x}\left(AD_x\frac{\delta T_w}{\delta x}\right) - \frac{1}{A}\frac{\delta}{\delta y}\left(AD_y\frac{\delta T_w}{\delta y}\right) - \frac{1}{A}\frac{\delta}{\delta x}\left(AD_z\frac{\delta T_w}{\delta z}\right) = \frac{W}{c_w\rho A}H_{sur} + \frac{p}{c_w\rho A}H_{bed} \quad (1)$$

where T_w is the water temperature (°C), t is the time (hour), x is the distance downstream (m), y and z are the longitudinal and vertical distance (m), A is the cross-sectional area (m^2), v_x, v_y, and v_z are mean water velocity in respective directions (m hr^{-1}), W is the river width (m), D_x, D_y, and D_z are the dispersion coefficients in respective directions (m^2 hr^{-1}), c_w is the specific heat of water ($4{\cdot}19 \times 10^{-3}$ MJ kg^{-1} °C^{-1}), ρ_w is the water density (1000 kg m^{-3}), p is the wetted perimeter of the river (m), H_{sur} is the total heat flux per area at the surface-water interface (W m^{-2}), and H_{bed} is the total heat flux per area at the streambed-water interface (W m^{-2}).

Table II. Selected periods for the river heat budget analysis at both Catamaran Brook and Little Southwest Miramichi River in 2007

Periods	Day of year	Dates	Hydrometeorological conditions
1	207–211	July 26–30	Highest water temperatures, high stream flow
2	222–226	August 10–14	Generally clear sky days
3	231–235	August 19–23	Relatively low flow
4	241–245	August 29–Sept. 2	High precipitation, cloudy days
5	247–251	September 4–8	Great variability in air and water temperatures
6	268–272	September 25–29	Autumn conditions

For river reaches of fairly uniform water temperature, the variability in water temperature along the river is usually small compared to temporal changes. In such cases, Equation (1) can be simplified for site specific conditions and the general one-dimensional model for vertically well mixed stream can be expressed as follows:

$$\frac{\delta T_w}{\delta t} = \frac{W}{c_w \rho A} H_{sur} + \frac{p}{c_w \rho A} H_{sed} \tag{2a}$$

In most rivers, when they are considered wide and shallow, the wetted perimeter (p) can be assumed to be equivalent to the surface river width (W) (e.g. Mackey *et al*., 1998). Therefore, the total heat flux at water surface (H_{sur}) and from the streambed (H_{bed}) can be expressed as the total heat flux (H_t) using the following equation:

$$\frac{\delta T_w}{\delta t} = \frac{W}{c_w \rho A} H_{total} \tag{2b}$$

where,

$$H_{total} = H_{sur} + H_{bed} = [H_s + H_l + H_e + H_c] + [H_b + H_g] \tag{3}$$

In Equation (3), H_s is the net short-wave radiation (W m^{-2}), H_l is the net long-wave radiation (W m^{-2}), H_e is the evaporative heat flux (W m^{-2}), H_c is the sensible heat flux (W m^{-2}), H_b is the streambed heat flux by conduction (W m^{-2}), and H_g is the streambed heat flux by groundwater flow (W m^{-2}). In the present study, Equation (3) will be used to estimate the total heat flux for the river and various fluxes are further described below.

The total heat flux was calculated by two different approaches in the present study. The first approach consisted of calculating the observed total heat flux or $H_t(O)$, whereas the second approach consisted of calculating the predicted total heat flux or $H_t(P)$. The observed total heat flux was calculated based on observed water temperature variability (i.e. calculating H_{total} from Equation (2b) based on actual changes in water temperature every hour, ΔT). The second approach consisted of calculating each heat flux component (every heat flux of Equation (3)), and then the summation of all fluxes represented the predicted total heat flux ($H_t(P)$). Both observed and predicted total heat fluxes were calculated and compared ($H_t(O)$ and $H_t(P)$).

Net short-wave radiation (H_s)

The net short-wave radiation is expressed as the difference between incoming and reflected solar radiation. The reflected radiation is usually estimated as 3% of the incoming solar radiation (Marcotte and Duong, 1973; Morin and Couillard, 1990; Caissie *et al*., 2007). Therefore, the net short-wave radiation can be estimated as follows:

$$H_s = 0{\cdot}97 H_{is} \tag{4}$$

where H_{is} represents the incoming solar radiation at the water surface (W m^{-2}) measured by a pyranometer.

Net long-wave radiation (H_l)

The net long-wave radiation includes the radiation emitted by the atmosphere, the water and the forest canopy and this form of radiation can be calculated using the Stefan-Boltzmann Law. The reflected atmospheric long-wave radiation was assumed at 3% of the incoming atmospheric long-wave radiation based on previous studies (Raphael, 1962; Morin and Couillard, 1990; Kim and Chapra, 1997; Evans *et al*., 1998). The emissivity of the long-wave radiation emitted by the water was 0·97 (Anderson, 1954). Most water temperature modelling studies have considered the net long-wave radiation; however, only a few studies have included the long-wave radiation emitted by the vegetation canopy (e.g. Rutherford *et al*., 1997). The long-wave radiation coming from the vegetation canopy can become important for stream with significant overhanging canopy such as Catamaran Brook. When considering the forest canopy, as well as other components of the long-wave radiation, the relationship is given by (Singh and Singh, 2001).

$$H_l = 0{\cdot}97\sigma \lfloor (FC + \varepsilon_a \times (1 - FC)) \times (T_a + 273)^4 - (T_w + 273)^4 \rfloor \tag{5}$$

where σ is the Stefan-Boltzmann constant ($5{\cdot}67 \times 10^{-8}$ W m^{-2} K^{-4}), FC is the forest cover factor (%), and ε_a is the atmospheric emissivity. In this equation, the forest temperature is assumed to be equal to that of air temperature with a forest emissivity of 0·97. The forest cover factor was estimated at 65% for Catamaran Brook (Cat Bk) and at 20% for the Little Southwest Miramichi (LSWM) based on field observations. The atmospheric emissivity was calculated by (Morin and Couillard, 1990).

$$\varepsilon_a = (0{\cdot}74 + 0{\cdot}0065 e_a) \times \left(1 + 0{\cdot}17 C^2\right) \tag{6}$$

where e_a is the air water vapour pressure (mm Hg), C is the cloud cover (clear sky (0), mainly clear (0·25), mostly cloudy (0·75) and total cloud cover (1)) and e_a can be computed using Equation (7).

$$e_a = 4{\cdot}583 \exp\left[\frac{17{\cdot}27T_a}{237{\cdot}3 + T_a}\right] \times \frac{RH}{100} \tag{7}$$

where RH represents the relative humidity (%).

Evaporative heat flux (H_e)

Mass-transfer methods (aerodynamic) are widely used in stream temperature modelling for the estimation of evaporation and the evaporative heat flux (Morin and Couillard, 1990; Sinokrot and Stefan, 1993; Webb and Zhang, 1997; Caissie *et al*., 2007). The evaporative flux equation can take the following form:

$$H_e = (a + bV) \times (e_s - e_a) \tag{8}$$

where a and b are empirical constants, V is the wind speed (m s^{-1}) and e_s is the saturated vapour pressure at the water temperature (mm Hg) and e_a is the water vapour pressure in the air (mm Hg). The empirical constants, a and b, were obtained by calibration for both study streams, in order to have evaporation rates close to those monitored within the study region (Canada's National Climate Archive, accessed 21 November 2008. http://www.climate.weatheroffice.gc.ca/), i.e. monthly lake evaporation between 2·5 and 4·0 mm during the summer), and substituting in Equation (8) we have

$$H_e = (6 + 3V) \times (e_s - e_a) \tag{9}$$

Sensible heat flux (H_c)

The sensible heat flux is the heat exchange that occurs at the air-water surface interface due to the temperature difference. As such, it is mainly a function of the difference between the air and water temperature and of wind speed. For this purpose, the Bowen ratio, Equation (10), was used (Bowen, 1926).

$$\frac{H_c}{H_e} = K\frac{(T_w - T_a)}{[e_s - e_a]}\frac{P}{1000} \tag{10}$$

where K is the proportionality constant (usually assumed as 0·61), and P is the atmospheric pressure (mm Hg). Substituting Equation (9) into Equation (10), the sensible heat flux equation becomes:

$$H_c = (3{\cdot}66 + 1{\cdot}83V)\frac{P}{1000}(T_a - T_w) \tag{11}$$

Precipitation heat flux (H_p)

In most water temperature modelling studies, the energy from precipitation has been assumed to be small (Webb and Zhang, 1997; Evans *et al*., 1998; Hannah *et al*., 2008). In this study, precipitation heat fluxes were considered as part of the energy heat budget to examine its relative contribution. The precipitation heat flux is a function of the difference between rainfall temperature and the stream water temperature. The precipitation heat flux was calculated from the equation provided by Marcotte and Duong (1973).

$$H_p = 1{\cdot}16y_p(T_p - T_w) \tag{12}$$

where y_p is the precipitation in mm, T_w the stream water temperature and T_p is the rain temperature (assumed equal to the air temperature in the present study, as was the case in Marcotte and Duong (1973)).

Streambed heat fluxes

To estimate the streambed heat flux, a water temperature advective-diffusion model (finite difference model) was calibrated for both Catamaran Brook (Cat Bk) and Little Southwest Miramichi River (LSWM). This model was calibrated using monitored intragravel temperatures at selected depths. When calibrated, the model was used to predict riverbed temperature profiles, $T(z, t)$ within the stream substrate using a one-dimensional advective-diffusion equation (Caissie and Satish, 2001)

$$k\frac{\partial^2 T_z}{\partial z^2} - v_g c_w \rho_w \frac{\partial T_z}{\partial z} = c_m \rho_m \frac{\partial T_z}{\partial t} \tag{13}$$

where T_z is the streambed temperature at depth z (°C), k_m is the thermal conductivity of the solid-fluid matrix (W m^{-1} °C^{-1}), v_g is the vertical velocity component (negative for upwelling water; m h^{-1}), c_m and ρ_m are the heat capacity (J kg^{-1} °C^{-1}) and density (kg m^{-3}) of the rock-fluid matrix, and z is the depth within the substrate (m).

To run the advective-diffusion model, data at both the upper and lower boundaries are required (i.e. at the streambed-water interface and at a specific depth within the substrate). Measured stream water temperatures were used for the upper boundary for both sites. Measured intragravel temperatures at a depth of 3 m in Cat Bk were used for the lower boundary for both rivers. The advective-diffusion model was run and temperatures were estimated at every 0·1 m (for depths 0 to 1 m) and every 0·2 m (for depths 1 to 3 m). For the purpose of this modelling, the vertical water velocity component (v_g) was assumed at 0·0025 m hr^{-1} for Cat Bk and 0·0020 m hr^{-1} for LSWM which is consistent with previous calibrations and field observations (D. Caissie, unpublished data). Based on water temperature observations within a groundwater well at Catamaran Brook, a constant groundwater temperature of 6·5 °C was assumed at a depth of 6 m into the substrate for Cat Bk and LSWM.

Heat capacity of the rock-fluid matrix (c) was estimated using the following equation:

$$\rho_m c_m = n\rho_w c_w + (1 - n)\rho_s c_s \tag{14}$$

where ρ_s and c_s are the density and specific heat capacity of the sediments at the streambed. The streambed consisted mainly of granite type rocks with a density (ρ_s) of 2578 kg m^{-3} and a specific heat capacity (c_s) of 775 J kg^{-1} °C^{-1}. The porosity (n) and the density of the

rock-fluid matrix (ρ_m) were estimated from field observations at the Cat Bk and at LSWM ($n = 0{\cdot}27$ and ρ_m 2300 kg m^{-3}). Therefore, the specific heat of the solid-fluid matrix (c_m) was calculated at 1130 J kg^{-1} °C^{-1}. The thermal conductivity of the saturated sediment k_m was calculated as a function of porosity n (0·27), and the thermal conductivity of water k_w (0·590 W m^{-1} °C^{-1}) and solids k_s (2·79 W m^{-1} °C^{-1}) using the following equation:

$$k = nk_w + (1 - n)k_s \tag{15}$$

With the above physical properties and porosity, the thermal conductivity of the saturated sediment (k_m) was calculated at 2·2 W m^{-1} °C^{-1} for Cat Bk and LSWM.

Streambed heat flux by conduction (H_b). The riverbed heat flux by conduction was estimated using the heat budget method (Hondzo and Stefan, 1994). This approach estimates the rate of variation in riverbed heat storage from temperature profiles at different depths and by comparing changes in heat storage over time. The streambed heat flux by conduction was calculated using the following equation:

$$H_b = (1/3600) \times \rho_m c_m \frac{\delta}{\delta t} \int_0^l T(z, t)dz \tag{16}$$

where $T(z, t)$ is the riverbed temperature profile with depth z at time step (t). The heat transfer was calculated from this equation as temperature changes through time.

Streambed heat flux by groundwater flow (H_g). The advective heat flux is both a function of the groundwater contribution (vertical velocity component) and the difference between surface water and groundwater temperatures. The advective heat flux was estimated using the formula provided by Sridhar *et al.* (2004).

$$H_g = \rho_w c_w Q_g (T_w - T_g) \tag{17}$$

where Q_g is the groundwater flow (m^3 s^{-1}) and T_g is the groundwater temperature at a certain depth close to the surface. Given the vertical flow component (v_g), the groundwater flow (Q_g) was then estimated for an area of 1 m^2. The vertical flow velocity was negative (for upwelling flow) in the original advection-diffusion heat transport Equation (13); however, upwelling flow becomes a positive discharge in Equation (17). To estimate the advective heat flux, the groundwater temperature (T_g) at 0·1 m from the previously calculated temperature profile of advective-diffusion model was used.

Modelling performance criteria

To evaluate the performance of the developed heat budget model, two criteria were used: the root-mean-square error (*RMSE*), and the coefficient of determination (R^2). The *RMSE* represents the mean errors associated to the model performance. It was calculated with the following equation:

$$RMSE = \sqrt{\frac{\sum_{i=1}^{N}(O_i - P_i)^2}{N}} \tag{18}$$

where N is the total number of hourly heat flux observations, O_i is the observed total heat flux (obtained from observed stream temperatures) and P_i is the predicted total heat flux.

The coefficient of determination (R^2) represents the percentage of variability that can be explained by the model. It was calculated with the following formula:

$$R^2 = \left[\frac{N\sum_{i=1}^{N} O_i P_i - \left(\sum_{i=1}^{N} O_i\right)\left(\sum_{i=1}^{N} P_i\right)}{\sqrt{\left[N\sum_{i=1}^{N} O_i^2 - \left(\sum_{i=1}^{N} O_i\right)^2\right] \times \left[N\sum_{i=1}^{N} P_i^2 - \left(\sum_{i=1}^{N} P_i\right)^2\right]}} \right] \tag{19}$$

with parameters being the same as in Equation (18).

RESULTS

Figure 2a) and b) show the hourly air and water temperature time series for the entire study period. Precipitation (hourly) and discharge (mean daily) for both Cat Bk and LSWM are presented in Figure 2c). Air temperatures were very similar within both stream microclimate environments (Figure 2a)). The mean air temperature at Cat Bk for the study period was 14·5 °C (−1·3 °C to 31·3 °C). The mean air temperature at LSWM was higher at 15·9 °C (−1·8 °C to 31·4 °C). Although microclimate air temperatures showed a similar pattern, water temperatures showed more pronounced differences between the two river systems (Figure 2b)). The maximum water temperature at Cat Bk occurred on day 206 (July 25) at 22·6 °C with an overall mean value of 14·4 °C (study period). Water temperatures were higher in LSWM, with a mean temperature of 18·8 °C, reaching a maximum of 28·7 °C (day 209; July 28). Discharge was higher in LSWM (average daily flow of 14·9 m^3 s^{-1}) than in the Cat Bk (average daily flow of 0·31 m^3 s^{-1}) due to the different size of these catchments. Hourly precipitation was measured at the Catamaran Brook meteorological station and is shown in Figure 1. The maximum hourly precipitation was recorded on August 8 (11·9 mm; day 220) whereas the maximum daily precipitation was recorded on July 5 (day 186; 24·9 mm; Figure 2c)).

The present study examined the differences between data from the remote meteorological station (Catamaran Brook Met Station - MetSta) with those measured at each of the sites. Table III shows average conditions for each of the Periods 1 to 6. In the present study, the Duncan's multiple range (DMR) test was used to differentiate differences among sites for each period (SAS 9·1·3). This test evaluates the statistical significance of ranges in the sorted sample for each pair of means using the studentized range statistic. Air temperatures were not significantly different between all sites during Periods

Table III. Comparison of period averages of specific meteorological parameter at the two microclimate sites (Catamaran Brook and Little Southwest Miramichi River) and at the meteorological station

Meteorological parameter	Site	Period					
		1	**2**	**3**	**4**	**5**	**6**
Air Temperature (°C)	**CatBk**[a]	21·3	16·0	11·5	14·4	13·4	12·3
	LSWM[b]	22·7	17·5	12·9	15·6	14·6	13·3
	MetSta[c]	22·8	17·6	12·5	15·4	15·3	13·8
Relative humidity (%)	**CatBk**	87·1	80·9	78·9	90·5	84·6	93·2
	LSWM	83·2	77·7	75·9	86·4	80·9	90·2
	MetSta	77·5	69·5	71·2	82·0	70·8	83·4
Wind speed (m/s)	**CatBk**	0·09	0·07	0·13	0·06	0·15	0·10
	LSWM	0·61	0·47	0·72	0·49	0·67	0·35
	MetSta	1·7	1·5	1·9	1·5	2·3	1·5
Incoming solar radiation (W/m^2)	**CatBk**	100	84·2	86·3	44·3	46·7	28·3
	LSWM	224	239	236	158	175	95·5
	MetSta	229	250	236	155	182	99·4
Water temperature (°C)	**CatBk**	19·1	16·2	12·9	15·0	13·2	12·2
	LSWM	23·9	20·3	16·6	18·4	16·4	14·8
Streamflow (m^3/s)	**CatBk**	0·516	0·180	0·098	0·246	0·092	0·125
	LSWM	21·1	14·3	8·90	13·7	9·10	7·70

[a] Catamaran Brook.
[b] Little Southwest Miramichi River.
[c] Meteorological station.

(3, 4, and 5; $p > 0{\cdot}11$) and no differences were noted between LSWM and the MetSta (all periods). Air temperature at CatBk was significantly different than LSWM and MetSta during Periods 1 and 2. Air temperature at Cat Bk was colder, although less than 2 °C. Relative humidity was significantly different between sites ($p < 0{\cdot}001$) and for all periods. Most of the difference was attributed to the MetSta. Relative humidity at LSWM and Cat Bk were higher than the remote meteorological station (MetSta). As expected, a significant difference was observed between sites for wind speed ($p < 0{\cdot}001$) for all periods. For instance, wind sheltering was dominant at the river microclimate sites with average wind speed of 0·06–0·15 m s^{-1} at Cat Bk, and 0·47–0·72 m s^{-1} at LSWM. The remote MetSta data showed higher wind speed (1·5–2·3 m s^{-1}). Incoming solar radiation measured at LSWM and at the MetSta was not significantly different ($p > 0{\cdot}05$) and averaged between 95·5 and 250 W m^{-2}. However, incoming solar radiation was significantly lower ($p < 0{\cdot}05$) at Cat Bk, with averages between 28·3 and 100 W m^{-2}. Although the air temperature was similar between Cat Bk and LSWM, the water temperature was significantly warmer ($p < 0{\cdot}001$) at LSWM by 3·5 °C on average. Water temperature varied between 12·2 and 19·1 °C at Cat Bk and, between 14·8 and 23·9 °C at LSWM (Periods 1–6). Table III also shows average discharge (for all periods) at Cat Bk and LSWM. As expected, discharge was significantly different between Cat Bk and LSWM ($p < 0{\cdot}001$).

Detailed analysis of river heat fluxes and water temperatures (Periods 1 and 6)

Heat fluxes related to precipitation were not illustrated on any of the figures because they were too small (compared to other heat fluxes); however precipitation heat fluxes were presented in Table IV for each period. In fact, precipitation fluxes contributed for less than 0·2 W m^{-2} at Cat Bk and 0·7 W m^{-2} at LSWM for Periods 1, 4, and 6 (Table IV).

Catamaran Brook water temperature and river heat fluxes (Period 1)

Air temperatures at Cat Bk during Period 1 (Figure 3a)) were high initially (day 207 to 209; peaked at 31·3 °C), and decreased thereafter (days 210–211; peaked at 23·2 °C). Water temperatures varied accordingly, between 17·1 and 22·6 °C. Total heat fluxes showed values ranging between −174 and 227 W m^{-2} during Period 1. The predicted total heat flux was overestimated during the daytime (day 207 and 208) while a good agreement was observed at night on those same days (Figure 3a)). A departure was observed between the two time series, $H_t(P)$ and $H_t(O)$, on day 210 coincidently with rainfall and high discharge event. Period 1 had the weakest relation between predicted and observed total heat flux with an RMSE of 61·3 W m^{-2} and a R^2 of 0·721 (Figure 3a); Table V).

When looking at the different components comprising the total heat flux ($H_t(P)$), it was noticed that the surface heat flux dominated the gains (positive fluxes) during the day and the losses at night (negative fluxes) whereas the streambed heat flux dominated the losses during the day with small gains at night (Figure 3b)). Surface heat flux experienced highest values early in Period 1 for both gains and losses (gains of 200–276 W m^{-2} and losses of −50·0 W m^{-2}; days 207–209) followed by lower values thereafter. Streambed fluxes were predominately losses throughout the period with values reaching −50·4 W m^{-2}. Slight gains were observed in early morning (reaching 17·5 W m^{-2} on day 210).

Table IV. Heat fluxes (gain, loss and net) for both river systems

		Catamaran Brook										
		$H_t(O)$	$H_t(P)$	H_{surf}	H_s	H_l	H_e	H_c	H_p	H_{bed}	H_b	H_q
Period 1	Gain	23·8	42·9	41·4	30·0	5·3	2·9	3·0	0·2	1·5	1·5	0·0
	Loss	−27·9	−8·6	−3·7	0·0	−1·6	−1·9	−0·2	−0·1	−4·9	−2·9	−1·9
	Net	−4·1	34·3	37·7	30·0	3·7	1·1	2·8	0·1	−3·4	−1·5	−1·9
Period 2	Gain	19·8	20·9	18·4	16·3	0·9	0·0	1·2	0·0	2·4	2·4	0·0
	Loss	−19·7	−22·9	−16·9	0·0	−8·0	−7·6	−1·3	0·0	−6·0	−4·1	−1·9
	Net	0·2	−2·0	1·6	16·3	−7·1	−7·6	0·0	0·0	−3·6	−1·7	−1·9
Period 3	Gain	15·7	21·2	17·0	15·5	0·5	0·0	1·0	0·0	4·2	3·9	0·3
	Loss	−16·8	−26·1	−21·4	0·0	−9·6	−9·6	−2·2	0·0	−4·7	−3·7	−1·1
	Net	−1·1	−4·9	−4·4	15·5	−9·1	−9·6	−1·2	0·0	−0·5	0·2	−0·7
Period 4	Gain	12·9	12·3	9·9	8·1	0·7	0·3	0·7	0·1	2·5	2·4	0·1
	Loss	−16·4	−16·8	−13·5	0·0	−7·5	−4·7	−1·2	−0·1	−3·3	−2·0	−1·3
	Net	−3·5	−4·4	−3·6	8·1	−6·8	−4·4	−0·5	0·0	−0·8	0·4	−1·2
Period 5	Gain	13·1	17·0	14·1	8·1	2·2	2·4	1·4	0·0	2·9	2·6	0·3
	Loss	−11·5	−18·4	−13·4	0·0	−6·4	−5·8	−1·2	0·0	−5·0	−3·8	−1·2
	Net	1·7	−1·4	0·7	8·1	−4·2	−3·4	0·2	0·0	−2·1	−1·2	−0·9
Period 6	Gain	8·2	11·3	9·5	5·8	1·2	1·6	0·9	0·1	1·8	1·7	0·1
	Loss	−8·9	−13·0	−10·1	0·0	−6·2	−3·0	−0·8	0·0	−2·9	−2·1	−0·8
	Net	−0·7	−1·7	−0·6	5·8	−5·0	−1·5	0·0	0·1	−1·1	−0·4	−0·7
		Little Southwest Miramichi River										
		$H_t(O)$	$H_t(P)$	H_{surf}	H_s	H_l	H_e	H_c	H_p	H_{bed}	H_b	H_q
Period 1	Gain	98·2	130·8	126·8	120·9	2·9	0·0	3·0	0·0	3·9	3·9	0·0
	Loss	−115·6	−59·0	−48·4	0·0	−22·7	−21·9	−3·2	−0·7	−10·5	−6·4	−4·2
	Net	−17·4	71·8	78·4	120·9	−19·8	−21·9	−0·2	−0·7	−6·6	−2·4	−4·2
Period 2	Gain	106·9	116·0	110·9	109·1	0·0	0·0	1·8	0·0	5·1	5·1	0·1
	Loss	−101·4	−87·8	−76·3	0·0	−45·4	−25·7	−5·2	0·0	−11·5	−8·0	−3·6
	Net	5·5	28·2	34·6	109·1	−45·4	−25·7	−3·4	0·0	−6·4	−2·9	−3·5
Period 3	Gain	93·5	105·5	96·9	96·3	0·0	0·0	0·7	0·0	8·5	8·0	0·5
	Loss	−90·7	−89·8	−79·7	0·0	−49·2	−24·2	−6·3	0·0	−10·0	−7·6	−2·4
	Net	2·8	15·7	17·2	96·3	−49·2	−24·2	−5·7	0·0	−1·5	0·4	−1·9
Period 4	Gain	66·5	76·5	70·8	70·0	0·02	0·00	0·7	0·1	5·7	5·6	0·2
	Loss	−79·0	−69·6	−63·3	0·0	−39·0	−18·8	−5·2	−0·3	−6·3	−4·1	−2·2
	Net	−12·5	6·9	7·5	70·0	−39·0	−18·8	−4·5	−0·2	−0·6	1·5	−2·0
Period 5	Gain	82·4	93·3	87·0	82·1	1·9	0·4	2·5	0·0	6·4	5·8	0·5
	Loss	−72·4	−63·5	−53·5	0·0	−33·3	−15·6	−4·6	0·0	−10·0	−7·5	−2·5
	Net	10·0	29·8	33·5	82·1	−31·4	−15·2	−2·1	0·0	−3·7	−1·7	−2·0
Period 6	Gain	47·2	53·9	49·0	43·7	2·1	1·6	1·5	0·1	4·9	4·6	0·3
	Loss	−50·6	−57·4	−51·4	0·0	−36·3	−10·8	−4·0	−0·2	−6·0	−4·3	−1·6
	Net	−3·5	−3·4	−2·3	43·7	−34·2	−9·3	−2·5	−0·1	−1·1	0·3	−1·4

Table V. Results of modelling performance between predicted total heat flux, $H_t(P)$, and observed total heat flux, $H_t(O)$

Period	Catamaran Brook		Little SW Miramichi River	
	RMSE (W/m^2)	R^2	RMSE (W/m^2)	R^2
1	61·3	0·721	130·8	0·922
2	34·1	0·792	85·4	0·943
3	30·3	0·875	72·6	0·947
4	23·2	0·819	64·2	0·947
5	24·8	0·836	82·6	0·915
6	17·7	0·806	55·8	0·910

Both surface and streambed heat fluxes were further analysed by calculating their different components (Figure 3c) and d)). For instance, the net short-wave radiation (H_s) was the major contributor to the surface heat gain during the day time (reaching 250 W m^{-2}; Figure 3c)). Also during the day, evaporative heat flux (H_e) was the main contributor of energy loss at the surface whereas, at night, it became positive (less than 19·1 W m^{-2}). The sensible heat flux (H_c) was smaller than most other components. Accordingly, the sensible heat fluxes varied between −4·0 W m^{-2} (at night) and 14·2 W m^{-2} (during the day). The net long-wave radiation was a major heat gain during the day (after solar radiation) and a major source of heat loss at night. The net long-wave radiation was generally between −27·7 W m^{-2} (at night) and 38·4 W m^{-2} (during the day). Hourly precipitation heat fluxes on day 209 and 210 varied between −5·0 and 8·7 W m^{-2} during this event with a total precipitation of 40 mm.

Heat flux by conduction was the dominant energy flux among the streambed fluxes (Figure 3d)). Streambed conduction provided heat at night (up to 18·0 W m^{-2}) and was the principal contributor of heat loss during

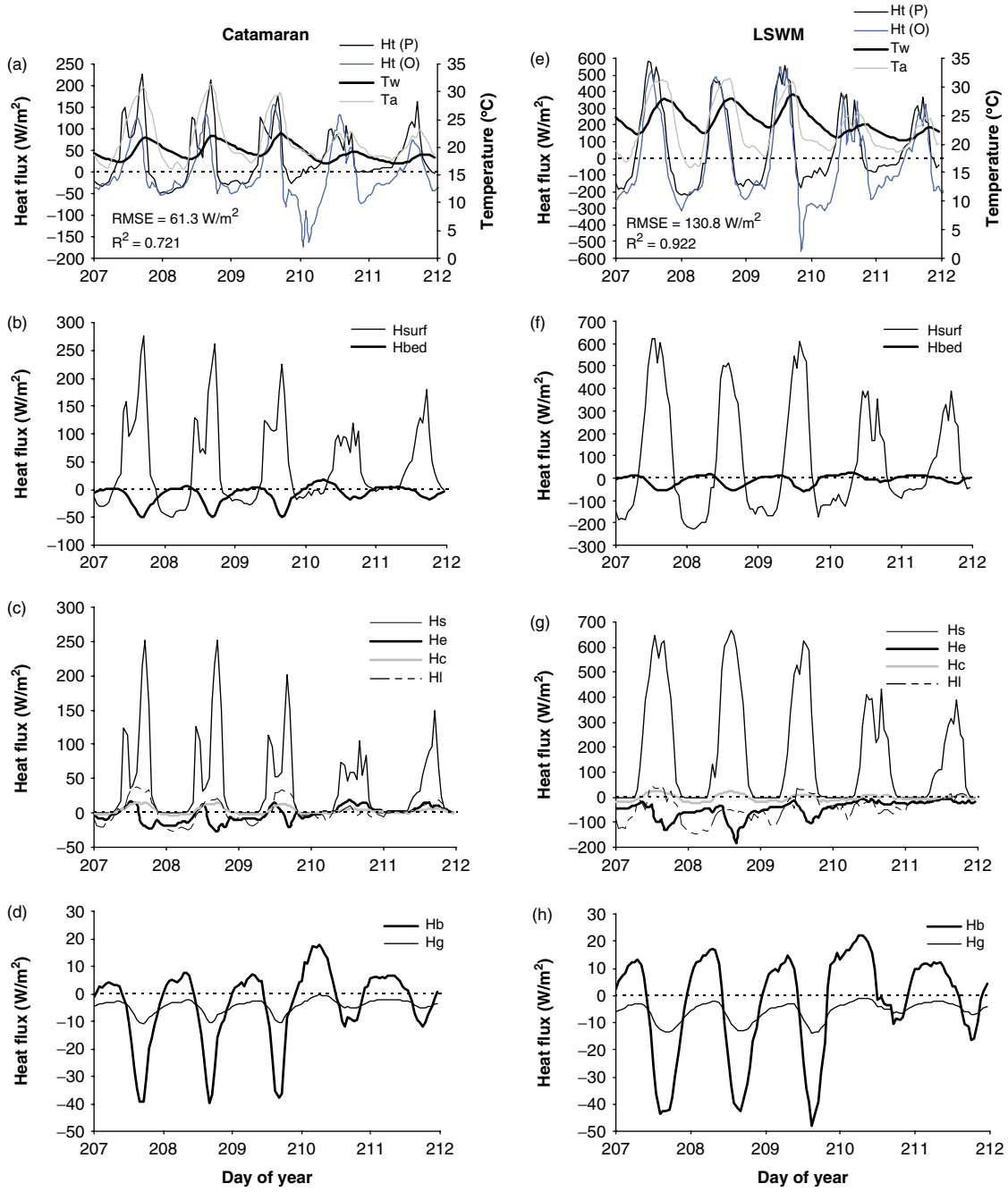

Figure 3. Detailed analysis of the different heat fluxes at both Catamaran Brook and Little Southwest Miramichi River during Period 1

the day (up to $-39{\cdot}9$ W m^{-2}). The advective heat flux was smaller than heat flux by conduction and generally remained negative throughout the study period ($-0{\cdot}5$ to $-10{\cdot}8$ W m^{-2}).

Heat gains and losses as well as the net heat fluxes are presented in Table IV (for all periods). For instance, the predicted total heat gain was calculated at 42·9 W m^{-2} compared to an observed value of 23·8 W m^{-2}. Heat losses showed significant differences as well (predicted = $-8{\cdot}6$ W m^{-2} and observed = $-27{\cdot}9$ W m^{-2}). Among the total fluxes during Period 1, the incoming solar radiation ($H_s = 30{\cdot}0$ W m^{-2}) dominated the gains whereas streambed fluxes (H_{bed}) dominated the losses ($-4{\cdot}9$ W m^{-2}).

Little Southwest Miramichi water temperature and river heat fluxes (Period 1)

Air temperatures at LSWM were similar to that of Cat Bk during Period 1 (Figure 3a) and e)) while water temperature varied between 20·7 and 28·7 °C (Figure 3e)). Both observed ($H_t(O)$) and predicted ($H_t(P)$) total heat flux had a similar pattern and good agreement between the two time series with the exception of day 209. Total heat flux at LSWM generally varied between -219 and 587 W m^{-2}; however there was a decline in the observed total flux during the night of day 209 (-552 W m^{-2}; Figure 3e)). Period 1 had the highest RMSE (130·8 W m^{-2}) and a comparable R^2 (0·922) to other periods (Table V).

Similar to Cat Bk, both surface and streambed heat fluxes were generally in opposite directions (Figure 3f)). Surface heat fluxes were higher in LSWM than in Cat Bk with peak values reaching from 386 to 625 W m^{-2}. Streambed heat fluxes in LSWM were very similar to those in Cat Bk and ranging from −62 to 21 W m^{-2}. Among the surface heat fluxes, the net short-wave radiation was observed to be the major heat gain (reaching 660 W m^{-2}), whereas evaporative fluxes and long-wave radiation were the most significant heat loss (reaching −183 W m^{-2}; Figure 3g)). Precipitation on days 209 and 210 resulted mainly as an energy loss and ranged between −51·6 and 5·5 W m^{-2}. The sensible energy flux contributed very little to the surface flux (−22·8 to 26·4 W m^{-2}). The streambed heat flux by advection only acted as an energy sink in LSWM and varying between −13·8 and −0·9 W m^{-2} (Figure 3h)). The streambed heat flux by conduction varied between −48·0 W m^{-2} (day) and 22·1 W m^{-2} (night).

Heat fluxes were also calculated for LSWM for each period (Table IV). Both observed and predicted total heat gain showed a noticeable difference during Period 1 (observed = 98·2 W m^{-2} and predicted = 130·8 W m^{-2}) with even greater differences for losses (observed = −115·6 W m^{-2} and predicted = −59·0 W m^{-2}). The surface heat flux (H_{sur}) was dominated by solar radiation gains (120·9 W m^{-2}) whereas losses were mainly due to the long-wave radiation (−22·7 W m^{-2}) and the evaporative flux (−21·9 W m^{-2}). Streambed fluxes represented a net loss (−6·6 W m^{-2}) of which the advective heat fluxes contributed −4·2 W m^{-2}.

Catamaran Brook water temperature and river heat fluxes (Period 6)

In order to contrast from the summer conditions during Period 1, Period 6 was also selected for a detailed analysis of heat fluxes (this period represents autumn conditions). An abbreviated presentation of Periods 2–5 will be in a subsequent section. As such, Period 6 had colder air temperature (4·8 to 22·2 °C) and the solar radiation was reduced compared to summer conditions (Table III).

Both observed and predicted total heat fluxes showed small variability during most days and values ranged between −52·6 and 85·0 W m^{-2} (Figure 4a)). During Period 6, a good agreement was observed between predicted and observed heat fluxes (RMSE = 17·7 W m^{-2}; R^2 = 0·806) and the total heat flux was almost neutral at night for most days. When looking at the surface *versus* streambed heat fluxes, fluxes were observed to be low as well (Figure 4c) and d)). For example, surface heat fluxes varied between −65·3 and 114 W m^{-2}, whereas streambed heat fluxes varied between −35·6 and 16·0 W m^{-2}. Peak fluxes from solar radiation during this period were less than 53·9 W m^{-2} (Figure 4c)). Precipitation heat flux was between −2·5 and 14·8 W m^{-2}. The streambed heat flux was still dominated by conduction (−29·5 to 14·1 W m^{-2}) and the advective heat flux was small (values ranging between −6·1 and 1·9 W m^{-2}; Figure 4d)).

Water temperatures were similar among days of Period 6 and varying between 10·0 and 14·6 °C. Total heat gains and losses were lower during Period 6 and of similar magnitude (Table IV). For instance, the predicted total heat gain was at 11·3 W m^{-2} (observed value = 8·2 W m^{-2}), whereas the total heat loss was −13·0 W m^{-2} (observed = −8·9 W m^{-2}). Although heat fluxes were small during Period 6, surface heat gains were dominated by solar radiation (5·8 W m^{-2}) and heat losses were dominated by the long-wave radiation (−6·2 W m^{-2}). The net streambed flux was −1·1 W m^{-2} and mainly dominated by advective heat fluxes (−0·7 W m^{-2}).

Little Southwest Miramichi water temperature and river heat fluxes (Period 6)

Water temperatures for LSWM during Period 6 were higher than in Cat Bk with values ranging from 11·6 to 18·3 °C (Figure 4e)). Similar to Cat Bk, water temperatures increased in LSWM during the first two days (day 268–269) and then generally decreased towards the end of the period.

Observed and predicted total heat fluxes showed good agreement (RMSE = 55·8 W m^{-2}; R^2 = 0·910) during Period 6 in LSWM (between −216 and 365 W m^{-2}). Surface heat fluxes were similar for most days (−207 to 383 W m^{-2}), with the exception of day 270–271 (showing lower peak heat gains <238 W m^{-2}; Figure 4f)). Surface heat fluxes were generally smaller than during Period 1 at LSWM reflecting autumn conditions. For instance, peak net short-wave radiation was between 217 and 349 W m^{-2} with the exception of day 272 where values reached 516 W m^{-2} (Figure 4g)). The net long-wave radiation was a major source of heat loss during Period 6 with values ranging from −149 W m^{-2}. Precipitation heat flux varied between −18·2 and 12·9 W m^{-2} over 2 days (day 270–271). Similar to Cat Bk, streambed heat fluxes were small. Heat flux by conduction varied between −33·9 to 21·0 W m^{-2} (Figure 4h)). The advective heat flux component was also relatively small (−7·7 W m^{-2} to 2·6 W m^{-2}).

Total heat gains and losses (observed and predicted) for LSWM showed good agreement during Period 6 (Table IV). The predicted heat gain was 53·9 W m^{-2} (observed value = 47·2 W m^{-2}), whereas the predicted heat loss was −57·4 W m^{-2} (observed value = −50·6 W m^{-2}). During autumn, heat grains were mainly from solar radiation (43·8 W m^{-2}), whereas heat losses were predominately from the net long-wave radiation (−34·4 W m^{-2}) followed by evaporative fluxes (−9·3 W m^{-2}). The streambed fluxes (H_{bed}) represented a net loss of −1·1 W m^{-2} for the period and was dominated by the advective heat fluxes (H_g = −1·4 W m^{-2}).

River heat fluxes and water temperatures (Periods 2–5)

Periods 2–5 were selected to represent a variety of microclimate conditions (Table II). Figure 5 shows observed ($H_t(O)$) and predicted ($H_t(P)$) total heat fluxes

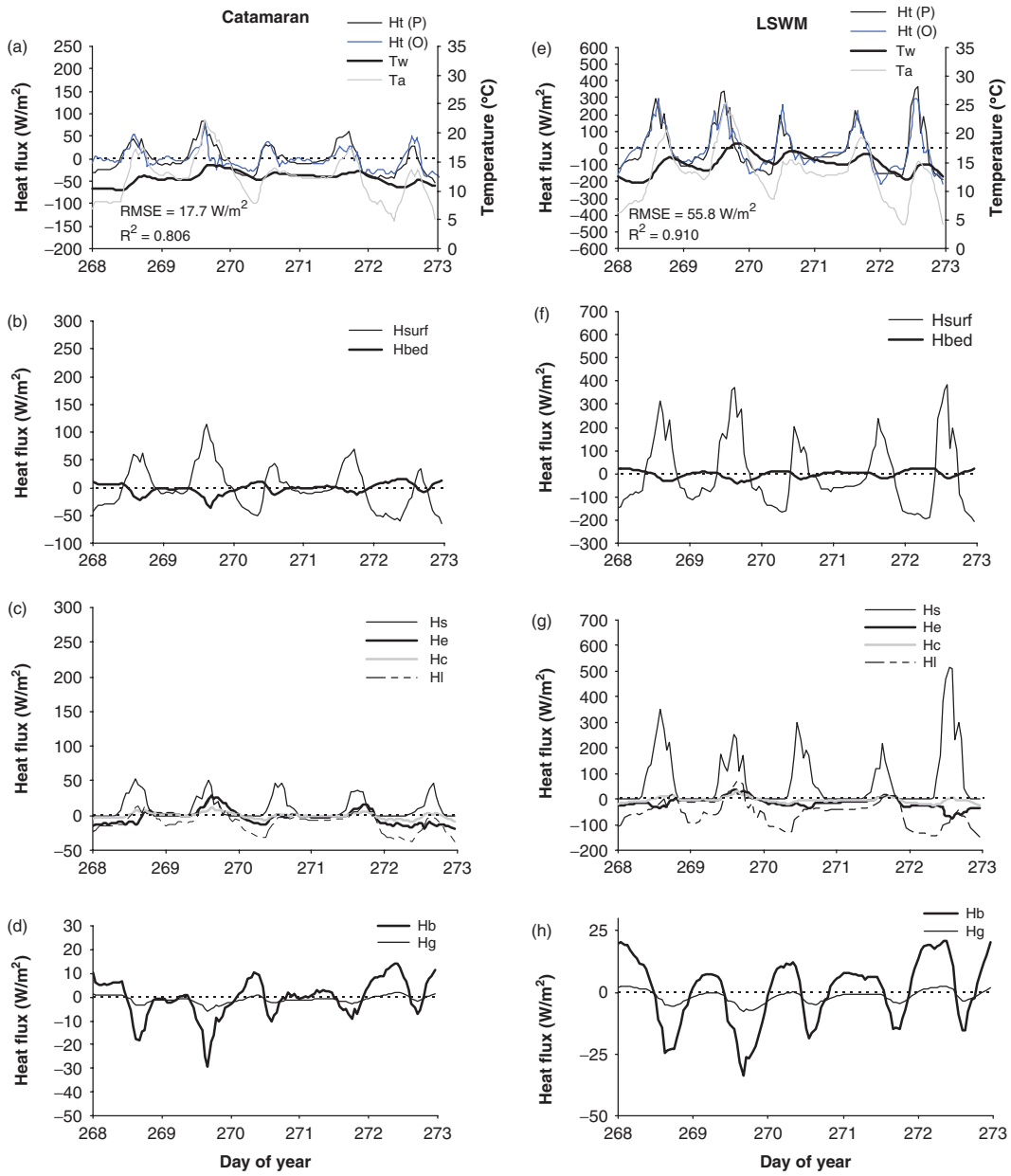

Figure 4. Detailed analysis of the different heat fluxes at both Catamaran Brook and Little Southwest Miramichi River during Period 6

for both Cat Bk and LSWM as well as air and water temperature time series, whereas Figure 6 shows the surface *versus* streambed contribution. A good agreement was seen between observed and predicted total heat flux during most periods, particularly for LSWM which also experiences larger variability (Figure 5). At Catamaran Brook, RMSEs ranged from 23·2 to 34·1 W m^{-2}, and R^2 were from 0·792 to 0·875. At LSWM, RMSEs ranged from 55·8 to 85·4 W m^{-2} and R^2 were higher than in Catamaran Brook with values over 0·915. Greater differences were noted in Cat Bk during Period 3, especially during daytime peak values and during the night time lows (Figure 5b)). The total heat flux generally varied from -72 W m^{-2} (night) with daytime high of 206 W m^{-2} at Cat Bk for all periods; however, with lower values during Periods 4 and 5 (Figure 5c) and d)). More variability in the total heat flux was observed for the LSWM (between -290 W m^{-2} and 620 W m^{-2}) than Cat Bk.

Both surface and streambed heat fluxes are presented in Figure 6 (for Periods 2–5). Similar to Periods 1 and 6, the surface fluxes were predominantly losses during the night and gains during the day. Surface fluxes varied between -84 and 246 W m^{-2} at Cat Bk, and between -244 and 634 W m^{-2} for LSWM. Surface heat gains were lower during some days of Periods 4 and 5 with correspondingly lower heat losses at night as well. Streambed fluxes were generally opposing the surface fluxes and predominately gains during the day and losses at night. Some periods, such as Period 4, showed low variability in streambed fluxes for both Cat Bk and LSWM. During most periods, streambed fluxes were similar between Cat Bk (-51 W m^{-2} to 28 W m^{-2}) and LSWM (-73 W m^{-2} to 33 W m^{-2}).

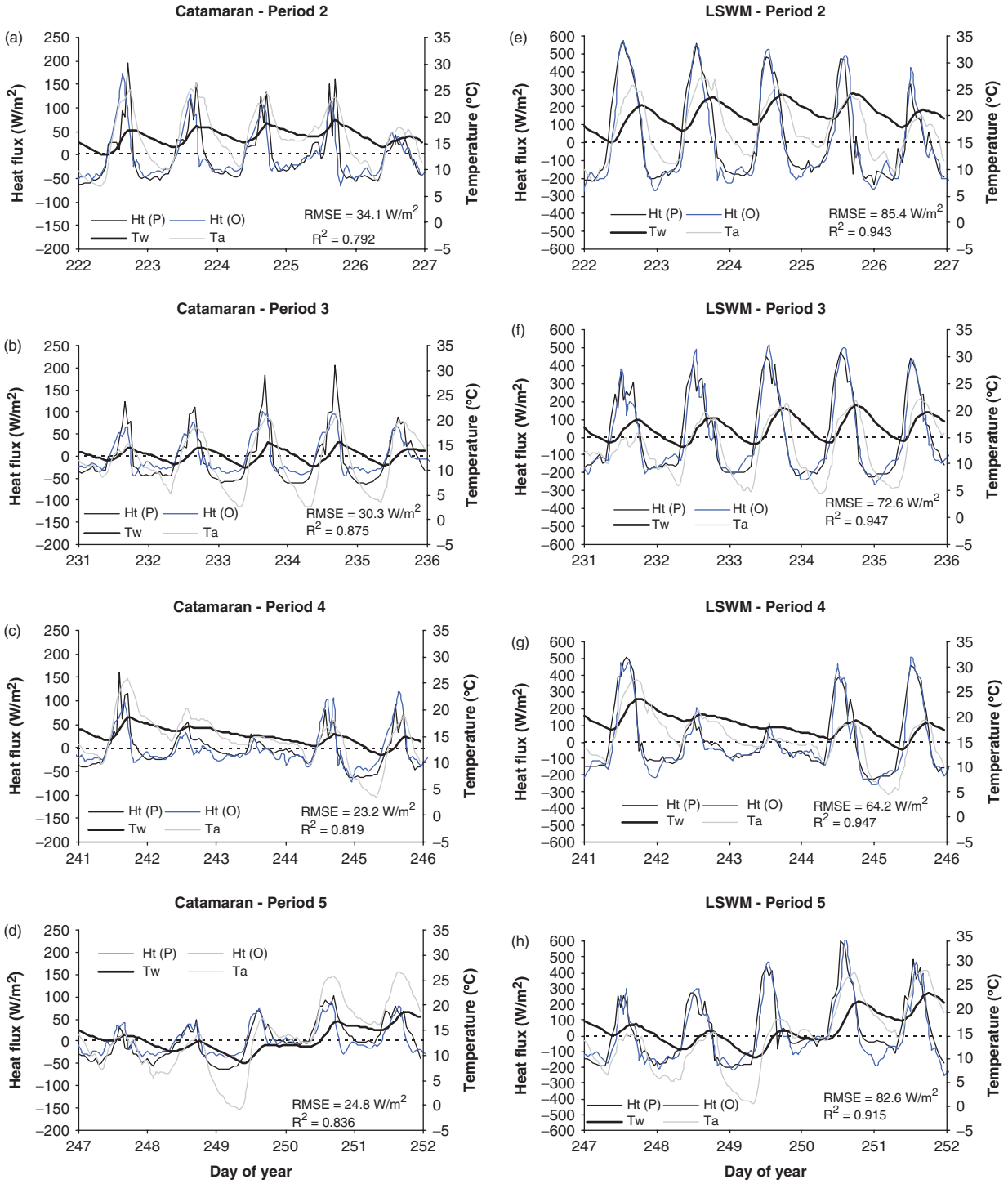

Figure 5. Results of the total heat flux (predicted *vs* observed) as well as air and water temperature time series for Catamaran Brook and Little Southwest Miramichi River for Periods 2–5

The different flux components are presented in Table IV for both Cat Bk and LSWM for Periods 2–5. For instance, surface gains were similar among periods (14·1–18·4 W m^{-2}, Cat Bk; 87–111 W m^{-2}, LSWM), with the exception of Period 4 which had a lower heat gain (9·9 W m^{-2}, Cat Bk; 71 W m^{-2}, LSWM). Surface heat losses generally varied between −21 and −13 W m^{-2} (Cat Bk) and −80 to −54 W m^{-2} (LSWM). It was also noted that surface gains (and losses) were more important in LSWM than Cat Bk. Streambed fluxes were similar between Cat Bk and LSWM although values in LSWM were slightly higher (both gains and losses). For instance, gains were on average 3·0 W m^{-2} at Cat Bk and 6·4 W m^{-2} for LSWM whereas losses were −4·8 W m^{-2} (Cat Bk) and −9·5 W m^{-2} (LSWM).

Comparison of total heat fluxes (observed vs predicted)

A comparison of observed *versus* predicted total heat gains and losses was carried out for both Cat Bk and LSWM for all 6 periods (Figure 7). It was observed that

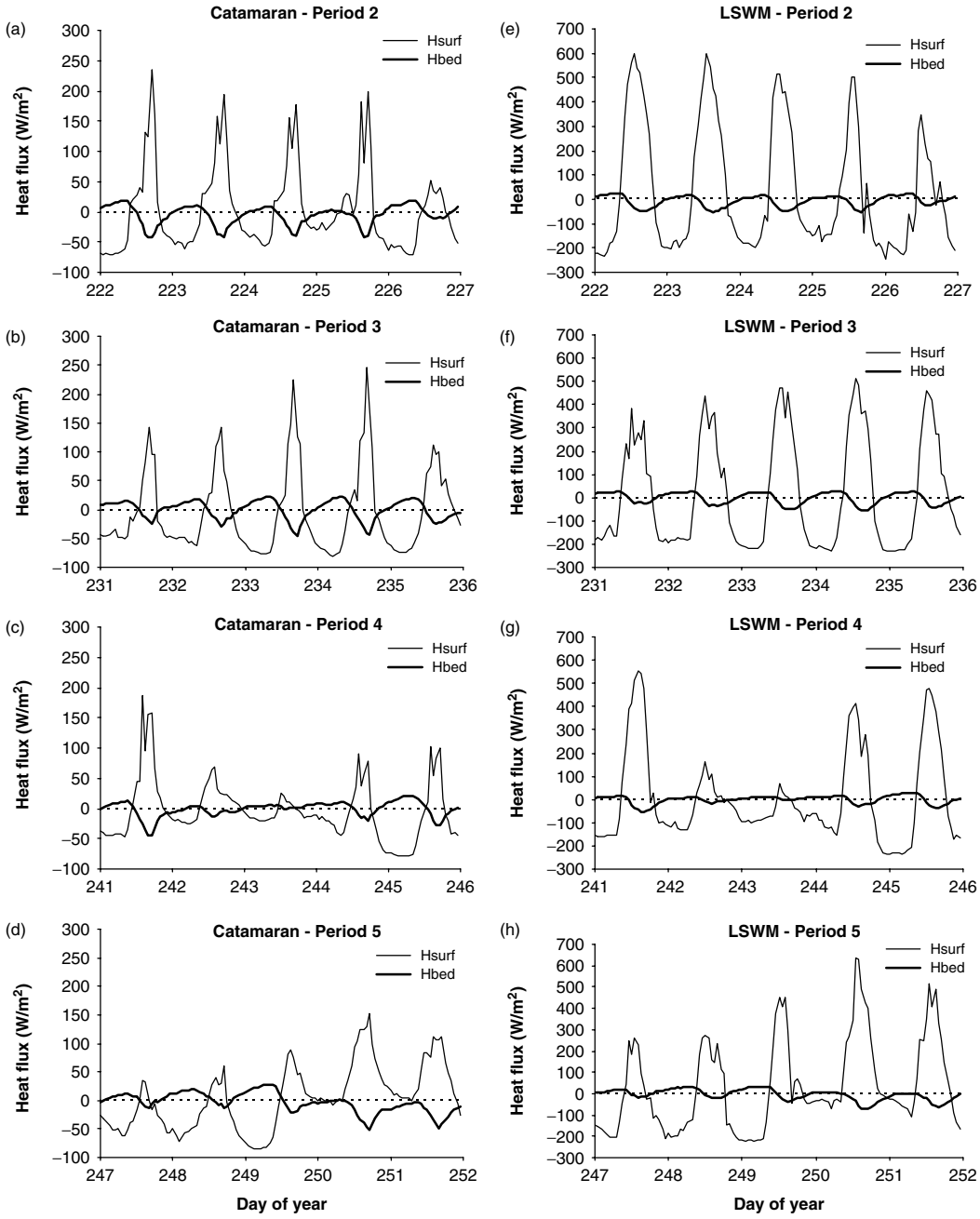

Figure 6. Results of the predicted surface and streambed heat fluxes at Catamaran Brook and Little Southwest Miramichi River for Periods 2–5

predicted heat gains and losses showed good agreement with observed fluxes for most periods with the exception of Period 1. In fact, during Period 1 heat gains were significantly overestimated whereas heat losses were underestimated for both Cat Bk and LSWM. For other periods, heat gains were well predicted for Cat Bk and even better for LSWM, whereas heat losses showed more variability between observed and predicted fluxes.

DISCUSSION

The present study implemented a deterministic water temperature model using near-stream microclimate data to better reflect heat exchanges occurring at the river level. This study also considered streambed heat fluxes in the modelling. Deterministic models permit a comparison of different fluxes and their relative contributions (Raphael, 1962; Morin and Couillard, 1990, Morin *et al.*, 1994). Results of this study are reflective of summer and autumn conditions (4 July–2 October), and therefore different results would be expected during other times of year (i.e. winter).

Results of the present study showed a clear difference between meteorological conditions at the remote site (MetSta) with those collected within the river environment (near-stream conditions at the microclimate sites; Table III). Differences (remote *vs* microclimate stations) were especially significant for solar radiation and wind speed whereas other parameters, such as air temperature and relative humidity, showed similar values. The LSWM

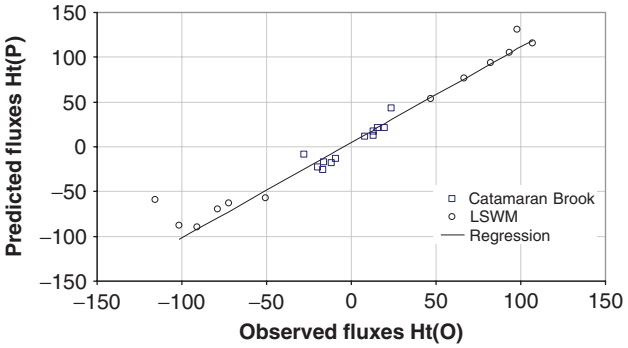

Figure 7. Predicted *versus* observed total heat fluxes (gains and losses) for each studies Periods 1–6 at Catamaran Brook and Little Southwest Miramichi River

site experienced higher solar radiation and wind speed than Cat Bk. Conversely, the relative humidity was 3 to 16% higher at Cat Bk (the more sheltered site) than at LSWM and the MetSta. Wind speed at Cat Bk was approximately 4–7% of values at the MetSta whereas LSWM showed values of 23–38%. Because wind speed plays such an important role in the evaporative and convective heat fluxes, only wind speed at the microclimate level will truly capture these fluxes. Similar observations can be made for solar radiation. At Cat Bk, incoming solar radiation was 27–44% of values observed at the MetSta and LSWM. With such differences between remote and microclimate sites, microclimate data are therefore important to capture near-stream heat fluxes, especially in smaller watercourses (Brown, 1969; Johnson, 2003; Johnson, 2004).

The analysis of different periods revealed varied heat flux conditions for both Cat Bk and LSWM (Figures 3–6). For example, results showed a good agreement between predicted and observed total flux (H_t) during most periods with the exception of Period 1 (Figure 7). It is expected that the precipitation event (40 mm of rain fell in over 10 h) played a role in Period 1. During this important rainfall event, the calculated precipitation fluxes (Equation 12) experienced both a gain (2·9 W m^{-2}) and a loss (−0·17 W m^{-2}) which could not explain the observed difference of almost −150 W m^{-2} to −200 W m^{-2}. Therefore, a significant heat loss was missing from this event which can only be explained by other processes. Heat fluxes may not have been added by direct precipitation falling into the river, but rather by advected heat flux inputs, like surface and near-subsurface hillslope pathways and groundwater (Brown and Hannah 2007). It was also found in other studies that the amount of heat added by a rainfall is highly dependant on the ambient atmospheric conditions (dew point, air temperature, solar radiation) before and after a storm event as well as the intensity and duration of the rainfall event (Herb *et al*., 2008). Owing to this large difference in fluxes, Period 1 will be excluded from the calculations when comparing mean fluxes of different periods.

When comparing flux contributions (Table IV), it was observed that the surface heat flux contributed 83% of the total energy gain and 77% of the energy loss at Cat Bk (excluding Period 1). The streambed flux at Cat Bk contributed 17% of the total energy gains and 23% of the losses. The surface heat flux was more important at LSWM (93% of the total energy gain and 88% of the total energy loss). The streambed flux at LSWM was much lower with gains of only 7% and losses of 12%. These results are consistent with those of Evans *et al*. (1998) who found that over 82% of the total heat exchange occurred at the air/water surface. Our study permits a comparison of different size rivers. A higher streambed contribution would also be expected for smaller streams than Cat Bk which would experience corresponding lower wind speed and solar radiation as well as higher groundwater contributions.

Solar radiation accounted for most of the daytime energy gain, as reported in previous studies (Webb and Zhang, 1997; Webb and Zhang, 1999; Younus *et al*., 2000; Webb and Crisp, 2006; Cozzetto *et al*., 2006; Caissie *et al*., 2007). In fact, solar radiation contributed on average 63% of the total heat gain at Cat Bk and 89% at LSWM. Solar radiation is very much a function of site conditions and predominately related to the degree of shading (Johnson, 2004). For instance, solar radiation was much lower at Cat Bk (up to 254 W m^{-2}) than at LSWM (up to 674 W m^{-2}). Both evaporative fluxes and long-wave radiation were predominately heat loss components. Evaporative flux losses were similar between Cat Bk (31%) and LSWM (25%) whereas the long-wave radiation flux losses were higher in LSWM (56%) than in Cat Bk (40%). The convective heat flux played a smaller role (generally less than 10% for both gains and losses) within the heat budget for both watercourses.

Only a few studies were found within the literature to have taken into account the long-wave radiation emitted from the forest canopy within the modelling study (e.g. Rutherford *et al*., 1997). As the forest cover becomes important, the incoming atmospheric long-wave radiation is replaced by the forest cover long-wave radiation. The long-wave radiation was usually found to be the main component of energy loss in most stream water temperature heat budgets along with evaporative fluxes. In our study, losses were more important at LSWM (52–63% of the total energy) than at Cat Bk (35–48%). Others studies (Evans *et al*., 1998; Webb and Zhang, 1997) showed long-wave radiation losses of 54 and 49% of the total energy which were closer to values for LSWM.

The evaporative heat flux was also a major source of energy loss (Table IV). At Cat Bk, heat loss accounted for 31% compared to 56% for LSWM. Notably, the major source of heat loss in Cat Bk was the long-wave radiation whereas in LSWM the major source of heat loss was the evaporative flux. Webb and Zhang (1997) showed that the evaporative heat flux can be an important source of energy loss with contributions reaching 30% of the total heat flux, values close to those observed in Cat Bk. Cozzetto *et al*. (2006) observed that the evaporation

tended to increase not only with wind speed but with stream temperatures as well.

The convective heat flux was relatively small with values (gains and losses) less than 3·0 W m^{-2} at Cat Bk, and less than 6·3 W m^{-2} at LSWM (Table IV). The convective heat flux at Cat Bk contributed similarly to the total heat flux gain (6%) and loss (7%). For LSWM, convective heat gains were relatively small (1%) compared to losses (7%). The convective heat fluxes were in general small compared to other heat fluxes (Caissie *et al*., 2007).

Most studies have neglected the precipitation heat flux within the modelling (e.g. Evans *et al*., 1998; Hannah *et al*., 2008) mainly because it contributed less than 1% of the daily heat budget (Webb and Zhang, 1997). In this study, precipitation heat fluxes were included; however, it contributed less than 1·2% to the total heat flux for both watercourses during periods with rainfall events (i.e. Periods 1, 4, and 6). Precipitation heat fluxes were less than 0·2 W m^{-2} at Cat Bk, and less than 0·7 W m^{-2} at LSWM (Table IV). Although the precipitation fluxes were relatively low compared to other fluxes, it was clear that the rainfall event during Period 1 had a significant cooling effect on water temperatures at both Cat Bk and LSWM (Figure 3a) and e)). Results suggest that the precipitation and corresponding flow generation processes most likely played an important role on water temperature dynamics that was not captured by the precipitation heat flux equations. For instance, concepts of streamflow generation, such as the variable area contribution (Freeze, 1974), most likely provided other sources of cold water to these watercourses than just direct channel precipitation during these rainfall events. More, research is needed to better understand water temperature dynamics in response to important rainfall events.

Studies have shown the importance of streambed fluxes in water temperature dynamics (Jobson, 1977; Jobson and Keefer, 1979; Sinokrot and Stefan, 1993; Moore *et al*., 2005). The streambed acted as an energy sink during the middle of the day and as an energy source later in the day and at night (Figures 3–6). For Cat Bk and LSWM, the most important streambed flux contribution occurred in late afternoon (e.g. 1500–1700 h) with losses reaching −50 W m^{-2}. The net streambed heat flux was predominantly an energy loss over the entire period at both Cat Bk (23%) and LSWM (12%) (excluding Period 1; Table IV) and may be attributed mainly to heat losses from the advective fluxes (H_q). In addition, the streambed contribution relative to the overall heat budget tended to be more important for smaller streams (20% at Cat Bk *vs* 10% for LSWM). Among the streambed fluxes, the heat flux by conduction was more important than the advective heat flux on a diel basis. In contrast, the streambed advective heat flux was much smaller than the flux by conduction during summer conditions. In autumn (e.g. Period 6) and during winter, conditions will be reversed. Water temperature variability will be significantly reduced and, therefore, the fluxes by conduction will be correspondingly low, whereas, the advective fluxes will still be present.

Predicted ($H_t(P)$) *versus* observed total heat flux ($H_t(O)$) showed slightly better results at LSWM than at Cat Bk (Figures 3–5) and correspondingly higher R^2 at LSWM. This was most likely related to the dominant surface heat fluxes at LSWM. It is expected that the estimation of surface heat fluxes has less uncertainties than corresponding streambed fluxes. Such results can be observed from Figure 7 where the LSWM (surface-dominated river) shows a better agreement between predicted and observed heat gains than Cat Bk (not considering Period 1). Heat gains in Cat Bk were slightly underestimated; presumably due to a lower solar radiation contribution. In fact, the main component of the heat gain for both sites was the solar radiation which was obtained by direct measurements (pyranometer). Figure 7 also suggests a better estimation of heat gains than losses (losses show more variability). Important component of heat losses, such as the evaporation rates (difficult to estimate), may have played an important role in higher uncertainties in the estimation of losses.

In conclusion, the present study showed the importance and the role of microclimate data to better estimate surface heat fluxes as well as the importance of the streambed flux contribution in the overall heat budget model. Results showed that for larger river systems surface heat fluxes are a dominant component of the heat budget with a correspondingly smaller contribution from the streambed. However, as watercourses become smaller and as groundwater contribution becomes more significant then the streambed contribution becomes an important component in the overall heat budget. With the exception of Period 1, predicted fluxes from the deterministic model showed good agreement to observed values. As such, deterministic models remain an effective tool in predicting the different heat flux components which will ultimately contribute toward a better understanding of river thermal regimes.

ACKNOWLEDGEMENTS

We would like to acknowledge the Natural Sciences and Engineering Research Council of Canada for funding the present research. The authors also thank the anonymous reviewers for their valuable comments and suggestions.

REFERENCES

Ahmadi-Nedushan B, St-Hilaire A, Ouarda TBML, Bilodeau L, Robichaud E, Thiémonge N, Bobée B. 2007. Predicting river water temperature using stochastic models: case study of the Moisie River (Québec, Canada). *Hydrological Processes* **21**(1): 21–34.

Anderson ER. 1954. Energy-budget studies, water-loss investigation: Lake Hefner studies. US Technical report, Professional Paper 269, Geological Survey: US Departement of Interior, Washington, DC; pp. 71–119.

Beitinger TL, Bennett WA. 2000. Quantification of the role of acclimation temperature in temperature tolerance of fishes. *Environmental Biology of Fishes* **58**: 277–288.

Bowen IS. 1926. The ratio of heat losses by conduction and by evaporation for any water surface. *Phys. Rev.* **27**: 316–355.
Bradley AA, Holly FM, Walker WK, Wright SA. 1998. *Journal of the American Water Association* **34**(3): 467–480.
Brown GW. 1969. Predicting temperatures of small streams. *Water Resources Research* **5**(1): 68–75.
Brown LE, Hannah DM. 2007. Alpine stream temperature response to storm events. *Journal of Hydrometeorology* **8**: 952–967.
Caissie D, El-Jabi N. 1995. Hydrology of the Miramichi River drainage basin. In *Water, Science, and the Public: the Miramichi ecosystem,* Chadwick EMP (ed.). *Canadian Special Publication of Fisheries and Aquatic Sciences* No. 123. NRC Research Press: Ottawa; 83–93.
Caissie D, Satish MG. 2001. Modelling water temperatures at depths within the stream substrate of Catamaran Brook (NB): potential implication of climate change. *Canadian Technical Report of Fisheries and Aquatic Sciences* **2365**: 27.
Caissie D. 2006. The thermal regime of rivers: a review. *Freshwater Biology* **51**: 1389–1406.
Caissie D, Satish MG, El-Jabi N. 2007. Predicting water temperatures using a deterministic model: Application on Miramichi River catchments (New Brunswick, Canada). *Journal of Hydrology* **336**(3): 303–315.
Cox TJ, Rutherford JC. 2000a. Thermal tolerances of two stream invertebrates exposed to diurnally varying temperature. *New Zealand Journal of Marine and Freshwater Research* **34**: 203–208.
Cox TJ, Rutherford JC. 2000b. Predicting the effects of time-varying temperatures on stream invertebrates mortality. *New Zealand Journal of Marine and Freshwater Research* **34**: 209–215.
Cozzetto K, McKnight D, Nylen T, Fountain A. 2006. Experimental investigations into processes controlling stream and hyporheic temperatures, Fryxell Basin, Antarctica. *Advances in Water Resources* **29**: 130–153.
Cunjak RA, Caissie D, El-Jabi N. 1990. The Catamaran Brook Habitat Research Project : description and general design of study. *Canadian Technical Report of Fisheries and Aquatic Sciences* **1751**: 14.
Evans EC, Mcgregor GR, Petts GE. 1998. River energy budgets with special reference to river bed processes. *Hydrological Processes* **12**: 575–595.
Freeze RA. 1974. Streamflow generation. *Rev. Geophys. Space Sci.* **12**: pp. 627–647.
Hannah DM, Malcolm IA, Soulsby C, Youngson AF. 2008. A comparison of forest and moorland stream microclimate, heat exchanges and thermal dynamics. *Hydrological Processes* **22**(7): 919–940.
Herb WR, Janke B, Mohseni O, Stefan HG. 2008. Thermal pollution of streams by runoff from paved surfaces. *Hydrological Processes* **22**: 987–999.
Hondzo M, Stefan HG. 1994. Riverbed heat conduction prediction. *Water Resources Research* **30**(5): 1503–1513.
Jobson HE. 1977. Bed conduction computation for thermal models. *Journal of the Hydraulics Division* **103**(HY10): 1213–1217.
Jobson HE, Keefer TN. 1979. Modelling highly transient flow, mass and heat transfer in the Chattahoochee River near Atlanta, Georgia. *Geological Survey Professional Paper* 11136. US Gov. Printing Office: Washington DC.
Johnson SL. 2003. Stream temperature: scaling of observations and issues for modeling. *Hydrological Processes* **17**: 497–499.
Johnson SL. 2004. Factors influencing stream temperatures in small streams: substrate effects and a shading experiment. *Canadian Journal of Fisheries and Aquatic Sciences* **61**: 913–923.
Kim KS, Chapra SC. 1997. Temperature model for highly transient shallow streams. *Journal of Hydraulic Engineering* **123**(1): 30–40.
Kinouchi T, Yagi H, Miyamoto M. 2007. Increase in stream tepmerature related to anthropogenic heat input from urban wastewater. *Journal of Hydrology* **335**: 78–88.
Macan TT. 1958. The temperature of a small stony stream. *Hydrobiologia* **12**: 89–106.
Mackey PC, Barlow PM, Ries KG. 1998. Relations between discharge and wetted perimeter and other hydraulic-geometry characteristics at selected streamflow-gaging stations in Massachusetts. US Geological Survey: *Water-Resources Investigations Report* **98**: 4094.
Marcotte N, Duong VL. 1973. Le calcul de la température de l'eau des rivières. *Journal of Hydrology* **18**: 273–287.
Markarian RK. 1980. A study of the relationship between aquatic insect growth and water temperature in a small stream. *Hydrobiologia* **75**: 81–95.
Moore RD, Spittlehouse DL, Story A. 2005. Riparian microclimate and stream temperature response to forest harvesting: a review. *Journal of the American Water Resources Association* **41**(4): 813–834.
Morin C, Nzakimuena TJ, Sochanski W. 1994. Prévision des températures de l'eau en rivières a l'aide d'un modèle conceptuel: le cas de la rivière Moisie. *Canadian Journal of Civil Engineering* **21**(1): 63–75.
Morin G, Couillard D. 1990. Predicting river temperatures with a hydrological model. In *Encyclopedia of Fluid Mechanic, Surface and Groundwater Flow Phenomena*, Vol 10, Cheremisinoff NP (ed). Gulf Publishing Company: Houston, Texas; pp. 171–209.
Morrill JC, Bales RG, Conklin MH. 2005. Estimating stream temperature from air temperature : Implication for future water quality. *Journal of Environmental Engineering* **131**(1): 139–146.
Morrison J, Quick MC, Foreman MGG. 2002. Climate change in the Fraser River watershed: flow and temperature projections. *Journal of Hydrology* **263**: 230–244.
Nagasaka A, Nakamura F. 1999. The influence of land-use changes on hydrology and riparian environment in a northern Japanese landscape. *Landscape Ecology* **14**: 543–556.
Nelson KC, Palmer MA. 2007. Stream temperature surges under urbanization and climate change: data, models, and responses. *Journal of the American Water Resources Association* **34**(2): 440–452.
Poole GC, Berman CH. 2001. An ecological perspective on in-stream temperature: natural heat dynamics and mechanisms of human-caused thermal degradation. *Environmental Management* **27**(6): 787–802.
Raphael JM. 1962. Prediction of temperature in rivers and reservoirs. *Journal of the Power Division* **88**: 157–181.
Rutherford JC, Blackett S, Blackett C, Saito L, Davies-Colley RJ. 1997. Predicting the effects of shade on water temperature in small streams. *New Zealand Journal of Marine and Freshwater Research* **31**(5): 707–721.
SAS. 9·1·3. *Statistical Analysis System*. SAS Institute Inc.: Cary, NC, USA.
Singh P, Singh VP. 2001. *Snow and Glacier Hydrology*. Kluwer Academic Publishers: Dordrecht, The Netherlands; p. 221.
Sinokrot BA, Stefan HG. 1993. Stream temperature dynamics: Measurements and modeling. *Water Resources Research* **29**(7): 2299–2312.
Sinokrot BA, Gulliver JS. 2000. In-stream flow impact on river water temperatures. *Journal of Hydraulic Research* **38**(5): 339–349.
Sridhar V, Sansone AL, LaMarche J, Dubin T, Lettenmaier DP. 2004. Prediction of stream temperature in forested watersheds. *Journal of the American Water Resources Association* **40**(1): 197–213.
Tung CP, Lee TY, Yang YC. 2006. Modeling climate-change impacts on stream temperature of Formosan landlocked salmon habitat. *Hydrological Processes* **20**: 1629–1649.
Webb BW, Zhang Y. 1997. Spatial and seasonal variability in the components of the river heat budget. *Hydrological Processes* **11**: 79–101.
Webb BW, Zhang Y. 1999. Water temperatures and heat budgets in Dorset chalk water courses. *Hydrological Processes* **13**: 309–321.
Webb BW, Crisp DT. 2006. Afforestation and stream temperature in a temperate maritime environment. *Hydrological Processes* **20**: 51–66.
Webb BW, Hannah DM, Moore RD, Brown LE, Nobilis F. 2008. Recent advances in stream and river temperature research. *Hydrological Processes* **22**(7): 902–918.
Wichert GA, Lin P. 1996. A species tolerance index of maximum water temperature. *Water Quality Resources Journal of Canada* **31**(4): 875–893.
Younus M, Hondzo M, Engel BA. 2000. Stream temperature dynamics in upland agricultural watershed. *Journal of Environmental Engineering* **126**(6): 518–526.

